Sintering and Characterization of WC-20wt.% (Fe,Co) Nano-Structured Powders Developed by Ball-Milling

Mi. Karbasi[a,*], Ma. Karbasi[a], A. Saidi[a], M. H. Fathi[a]

[a] *Department of Materials Engineering, Isfahan University of Technology, Isfahan, Iran.*

ARTICLE INFO

Article history:

Received 23 Apr. 2014
Accepted 16 May 2014
Available online 31 Aug. 2014

Keywords:

WC-based cemented carbides
Ball milling
Microstructure
Hardness
Sintering

ABSTRACT

The aim of the present work is to study the effects of the nanostructured WC-20 wt. % (Fe,Co) with different iron to cobalt ratios on microstructure and hardness of the sintered samples. Furthermore, a sample with a cobalt binder was produced under the same conditions for comparison purposes. The nanocomposite development, after different milling times, was monitored by X-ray diffraction (XRD), scanning electron microscopy (SEM), and transmission electron microscopy (TEM). A homogenous distribution of nanostructured WC (crystallite size less than 30 nm) in the binder matrix was formed after 25 h of milling. The hardness and the relative density of the WC-20wt. % (Fe,Co) composites consolidated by conventional sintering at 1350˚C were investigated. In the sintered samples after 25 h of milling, tungsten carbide grains have a uniform distribution with a lower grain size. Densification and hardness improved after 25 h of milling and reached optimum levels for the 25 h milled powders with equal ratio of iron to cobalt.

1. Introduction

A high volume fraction of the hard WC phase and a ductile binder is the major constituent of WC-based cemented carbides. Extreme hardness, high elastic modulus, and flexural strength over other materials make them useful as cutting tools, rock drills, punches, extrusion, pressing dies, and wear-resistant coatings [1, 2].

The properties of cemented carbides can be improved by appropriate modification of microstructure (e.g. the WC grain size) or microchemistry (e.g. composition of binder).

On the one hand, mechanical properties of hard metals seem to rely on microstructures while affected by the microstructure of WC powders. A key feature is that the toughness and the hardness increase simultaneously with the refining of WC [3]. Thus, there has been a great effort to study the development of nanostructured hard metals. Although numerous techniques have been developed to produce nanostructured materials, mechanical alloying has turned out to be a popular method to produce nano crystalline materials due to its simplicity, relatively inexpensive equipment, and its potential for large-scale production [1].

On the other hand, even though WC-Co

Corresponding author:
E-mail address: m.karbasi@ma.iut.ac.ir (Minoo Karbasi).

composites are the most important commercial grade of cemented carbides, because of their disadvantages such as the Co toxicity and high and variable market value, considerable efforts have been made for replacing Co by other binders such as iron, nickel and their compounds [4-6], intermetallics [7, 8], and stainless steels [9, 10] to improve the properties of WC based composites. Prakash [11] reported that cemented carbides with Fe-rich binders had enhanced properties such as higher hardness, abrasive wear resistance, toughness, and strength properties compared with Co-bonded hard metals. Other researchers also reported similar and superior values for hardness, toughness, and transverse rupture strength (TRS) of the Fe-rich binder over the WC–Co system [12-14]. Wittmann et al [4] reported that the nature of the binder changes the growth behavior by influencing the metal-to-carbon bond relationship. In this regard, iron has the highest affinity to carbon compared to cobalt and nickel, so it can form metal-carbon bonds (as in liquid phase), resulting in masking the carbon, and impeding carbon transport and precipitation by increasing the activation energies of the nucleation and growth processes. This seems to be a possible explanation for the extremely low coarsening rate of the WC in case of the iron binder (through bond formation), compared with the WC–Co and WC–Ni systems [4]. Moreover, iron has good wettability and solubility for WC [15] and ternary eutectic temperature lower than Co [16].

The purpose of this study is, therefore, to evaluate the influence of the nanostructured WC-20 wt.% (Fe,Co) with different ratios of iron to cobalt (or Fe:Co) on the microstructure and hardness of the WC-based cemented carbide processed by powder metallurgy.

2. Experimental

2. 1. Starting materials

High purity (>99.5%, Merck, Germany) starting materials (WC, Co, Fe) were used for the preparation of composites. The SEM micrographs of the starting powders are shown in Fig.1.

2. 2. Composite preparation

The nominal compositions of the materials studied in the present study are given in Table 1. It should be mentioned that sample A with a cobalt binder was produced under the same conditions for comparison purposes. The milling of the samples as illustrated in Table 1 was performed in a planetary ball mill under an argon atmosphere for 15 min, 5, 10, and 25 h. The ball-to-powder weight ratio and the rotational speed were 20:1 and 500 rpm, respectively. Green bulk samples were prepared by cold-pressing the powder mixtures in a cylindrical steel die. For all of the samples, the compaction pressure was 500 MPa.

2. 3. Sintering and characterization

Sintering was performed at 1350˚C, for 60 minutes under hydrogen atmosphere controlled by hydrogen generator model SHC-300. The heating rate was 10 ˚C min−1. The density of the sintered parts was determined by water displacement (Archimedes) method. The samples for metallographic study were prepared according to ASTM B665. The structure of the samples was characterized by a Philips X'PERT MPD X-ray diffractometer (Cu Kα radiation: λ= 0.154 nm at 20 kV and 30 mA). Powder morphology and microstructure developments were examined using a Philips XL30 scanning electron microscope (SEM) at an accelerating voltage of 30 kV with an energy dispersive X-ray spectrometer (EDS). Vickers hardness of the compacts was measured at a load of 293 N (HV30) and dwell time of 10 s.

3. Results and Discussion

3. 1. Characterization of the milled WC-Fe-Co powder

Fig. 2 shows the X-ray diffractograms of the samples as indicated in Table 1 after different milling times. As can be seen in all patterns, the starting powders contain Fe, Co, WC, and small amounts of W_2C phase. It should be noted that Co phase is composed of fcc (α) and hcp (ε) phases. The hcp-Co phase which is stable at room temperature is transformed into fcc-Co at temperatures around 417 ° C with reversible martensitic transformation [17]. This martensitic transformation also occurs under stress condition [18]. In fact, the cold work on

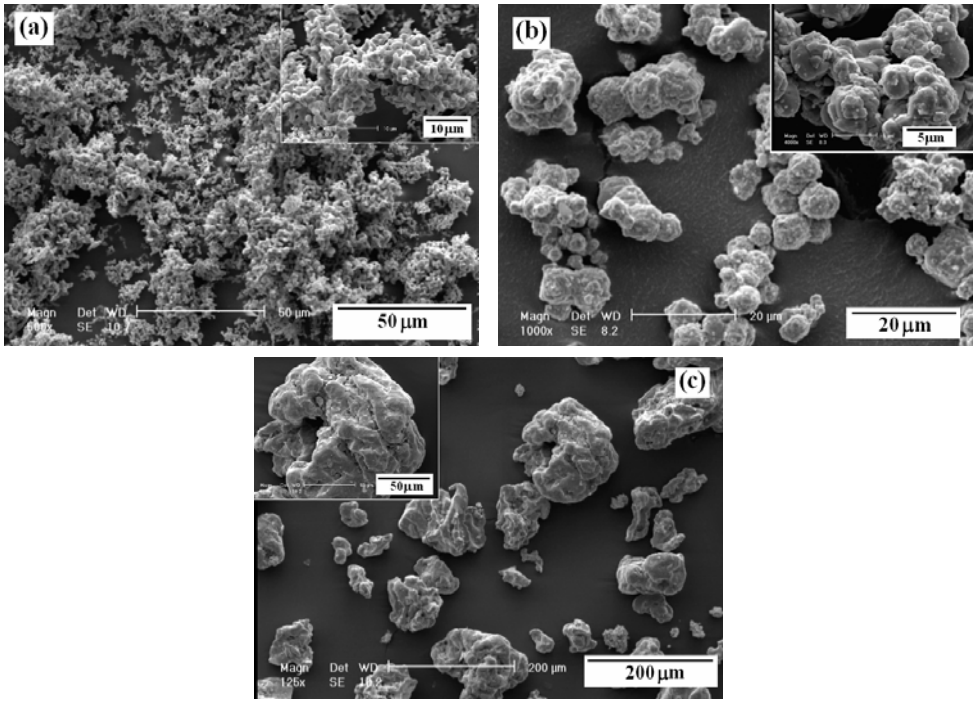

Fig. 1. SEM micrographs of the starting powders: (a) Co, (b) WC and (c) Fe

Table 1. The nominal compositions of the samples

Sample code	Composition
A	Co-80%WC
B	Fe/Co: 2/8 – 80% WC
C	Fe/Co: 1/1 – 80% WC
D	Fe/Co: 7/3 – 80% WC

the fcc-Co phase during mechanical alloying can provide the required energy for this transformation [17, 19].

After 5 hours of milling, disappearance of Co peaks can be explained by dissolution of Co into Fe (bcc structure) in order to form the (Fe,Co) solid solution, as shown elsewhere [20, 21]. Increasing the milling time is accompanied by line broadening and a steep decrease in the intensity due to the decrease of grain size and increase of internal strain as a result of milling.

The crystallite size of the powder during milling can be determined from the broadening of XRD peaks by Williamson–Hall equation (Eq. 1) [22, 23]:

$$B\cos\theta = 0.9\frac{\lambda}{D} + \varepsilon \sin\theta \qquad [1]$$

Where B is the full-width at half maximum intensity, λ is the wavelength of the X-ray used, D is the average crystallite size, θ is the Bragg angle, and ε is the average strain. The crystallite size and the internal strain of the WC phase of the samples were calculated from the line width shown in Fig. 3 as a function of MA time. In all samples, the crystallite size of WC decreased sharply to less than 30 nm after 10 h of MA, but further refinement of the crystallite size occurred gradually after 25 h of MA. It should be note that the internal strain in all samples increased over 1.1 percent after 25 h of MA. The reduction of crystalline size during milling process can be due to the following reasons:

1. The localization of plastic deformation (in the form of shear bands containing a high density of dislocations).
2. Formation of cells and subgrains by annihilation of dislocations.
3. Conversion of subgrains into grains through mechanically driven grain rotation and subgrain boundary sliding [23].

As the XRD behavior of the samples is similar, one of the samples (sample C) was chosen to investigate microscopy characterization. Morphology of the MA powders after different milling times of sample C is shown in Fig. 4. Fig. 5 presents the cross

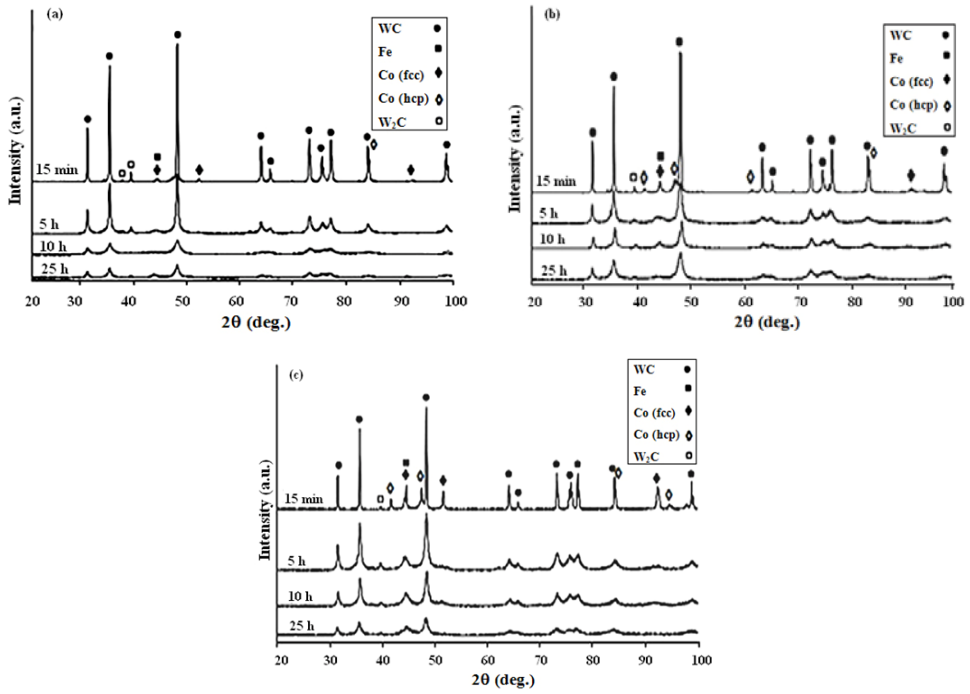

Fig. 2. X-ray diffractograms of samples (a) B, (b) C, and (c) D after different milling times

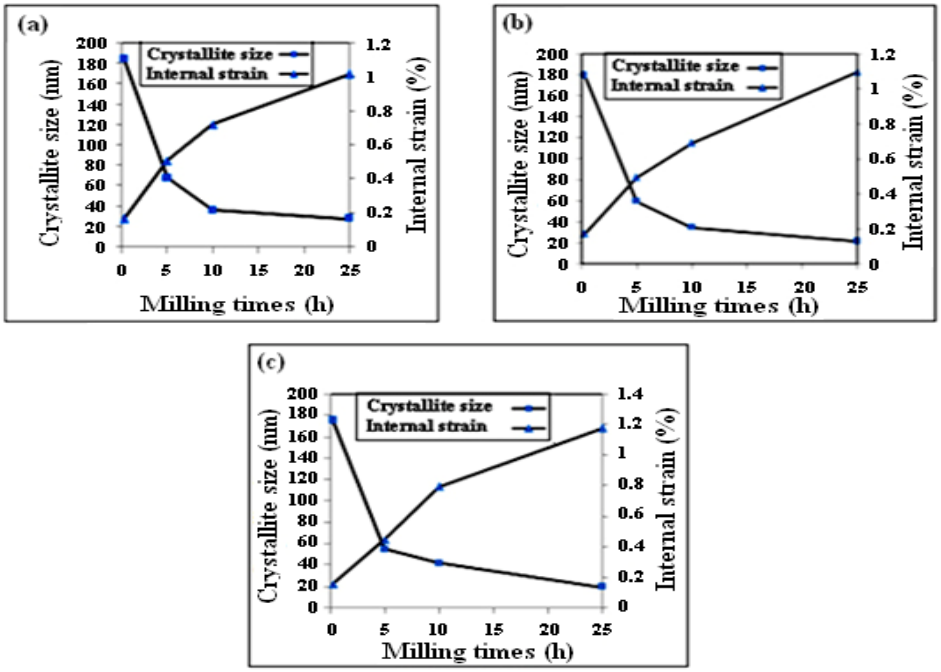

Fig. 3. The crystallite size and the internal strain of WC phase of samples (a) B, (b) C, and (c) D at different milling times

sectional SEM micrographs of the development of the nanocomposite particles (sample C) with milling time. During the MA process, the powders were subjected to high-energy collision, which caused plastic deformation, cold welding, and fracture of the powders. Plastic deformation and cold welding are predominant during the initial stage of ball milling in which deformation and cold welding lead to a change in particle shape and size [1].

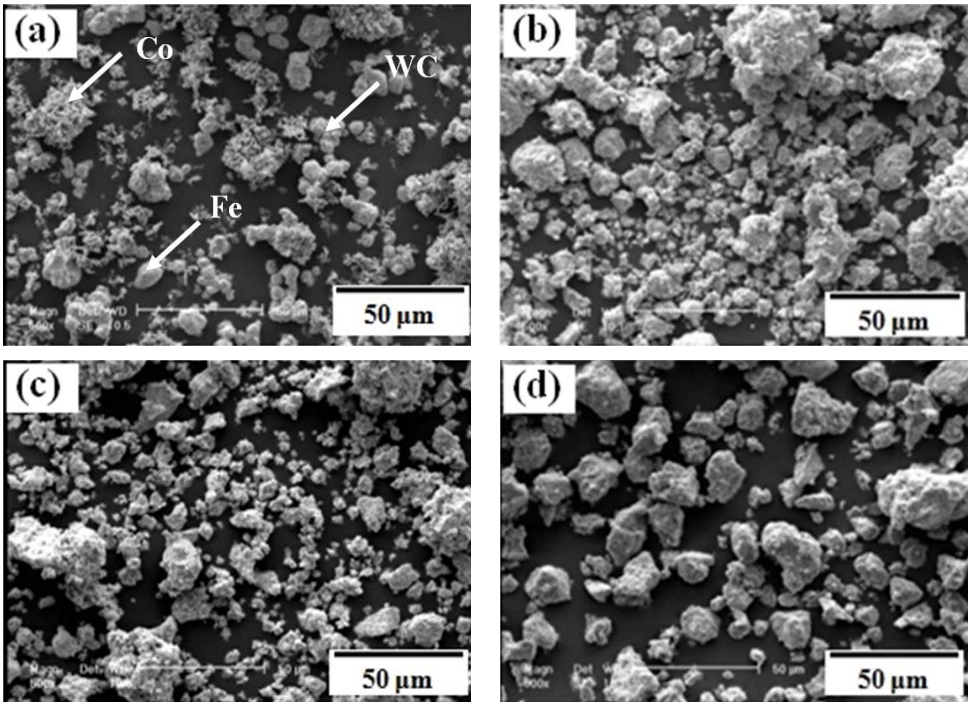

Fig. 4. Morphology of the WC-20wt.%(Fe,Co) composite particles at different milling times: (a) 15 min, (b) 5 h, (c)10 h and (d) 25 h

From Fig. 4(a), it can be observed that Fe, WC, and Co particles are individually distinguishable. Furthermore, in Fig 5(a), based on the EDS analysis results, WC, Fe, and Co particles are shown in white, light grey, and dark grey colors, respectively. As a result, after milling for 15 min, only a partially physical mixture was formed and the Fe, Co and WC powders exhibited different particle distributions. Although after 5 h of milling, the particles are not individually distinguishable, Fig. 4(b) and Fig. 5(b) show that a quantity of hard WC particles which decrease in size are embedded into the binder. Morphology of the powders after 10 h of milling (Fig. 4(c)) shows that, in this stage fracturing becomes a significant process, which leads to a decrease in particle size. At this stage, particle agglomeration is also evident. According to Fig. 5(c), there are WC particles which are not completely embedded into binder (white arrows). Fig. 4(d) indicates that the particle size of nanocomposite powders increases because the predominant mechanism after 25 h of milling is cold welding. With the decrease of fragment size, the tendency to aggregate increases, thereby causing fracture resistance increase. Particle fineness approaches a limit as the milling continues and maximum energy is expended [20]. As illustrated in Fig. 5 (d), a homogeneous distribution of fine WC grains in the binder matrix was formed after 25 h of milling. As illustrated in these figures, three important changes occur:

1. Considerable refinement and reduction in particle size can be seen.
2. Hard particles of WC encapsulated into (Fe, Co) solid solution create the WC-(Fe, Co) composite.
3. The hard WC particles become finer. They are distributed more uniformly in the matrix after 25 hours of milling.

Fig.6 shows the SE-SEM micrograph for the cross-sectional view of the composite powders (sample C) after 25 hours of ball milling (Fig. 6(a)) and elemental X-ray maps of W (Fig. 6(b)). Tungsten X-ray map shows the uniform distribution of tungsten carbide particles in the binder, confirming the formation of a homogeneous composite. TEM image of the 25 h milled powder presented in Fig. 7 reveals a homogenous dispersion of reinforcements with the size of about 20 nm in the matrix.

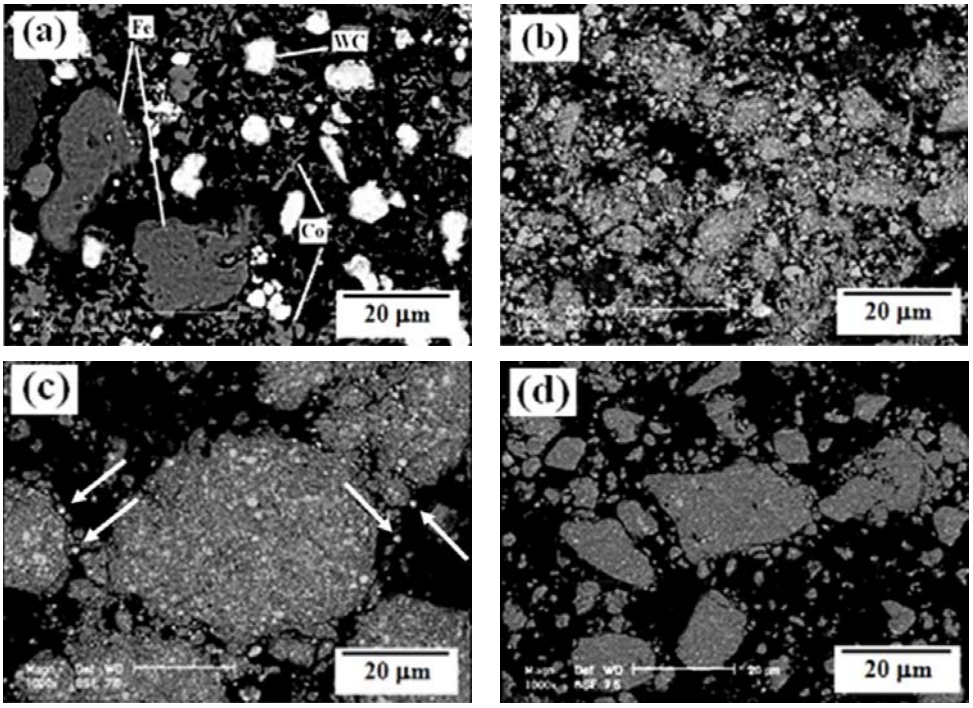

Fig. 5. The cross-sectional BSE-SEM micrographs of the WC-20wt.%(Fe, Co) composite particles at different milling times: (a) 15 min, (b) 5h, (c)10 h and (d) 25 h

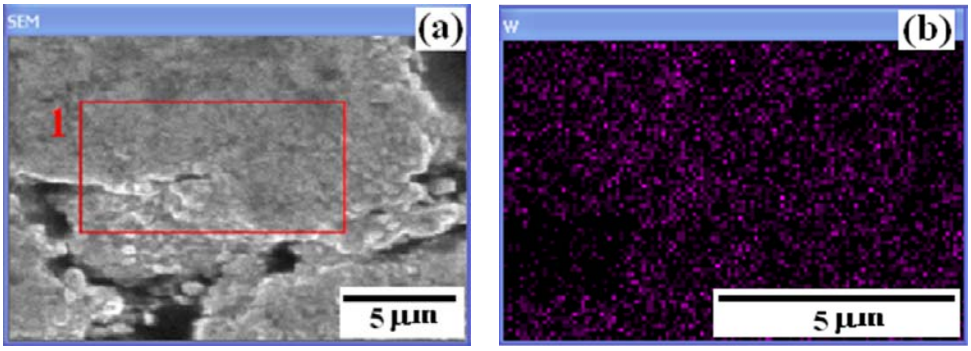

Fig. 6. (a) The cross-sectional SE-SEM micrographs of the WC-20wt.%(Fe,Co) composite particles, (b) Elemental X-ray maps of tungsten from the cross section of powders after 25 hours of milling

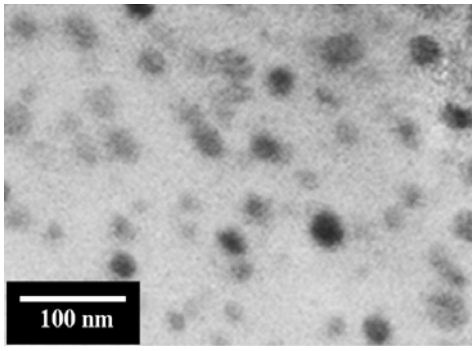

Fig. 7. TEM image of the 25 h milled powder (Sample C)

As a homogeneous distribution of fine WC grains in the binder matrix was formed after 25 h of milling, microstructure of other samples are shown in Fig. 8. It is evident that in all samples nanocomposite is formed after 25 h of milling.

3. 2. Characterization of the sintered WC-Fe-Co composite

In order to investigate the sintering behavior of the milled powders, the samples as listed in Table 2 were compacted and sintered at 1350˚C. Fig. 9 indicates the changes in relative density of the sintered composites after 15 min and 25 h of milling. As can be seen, increasing

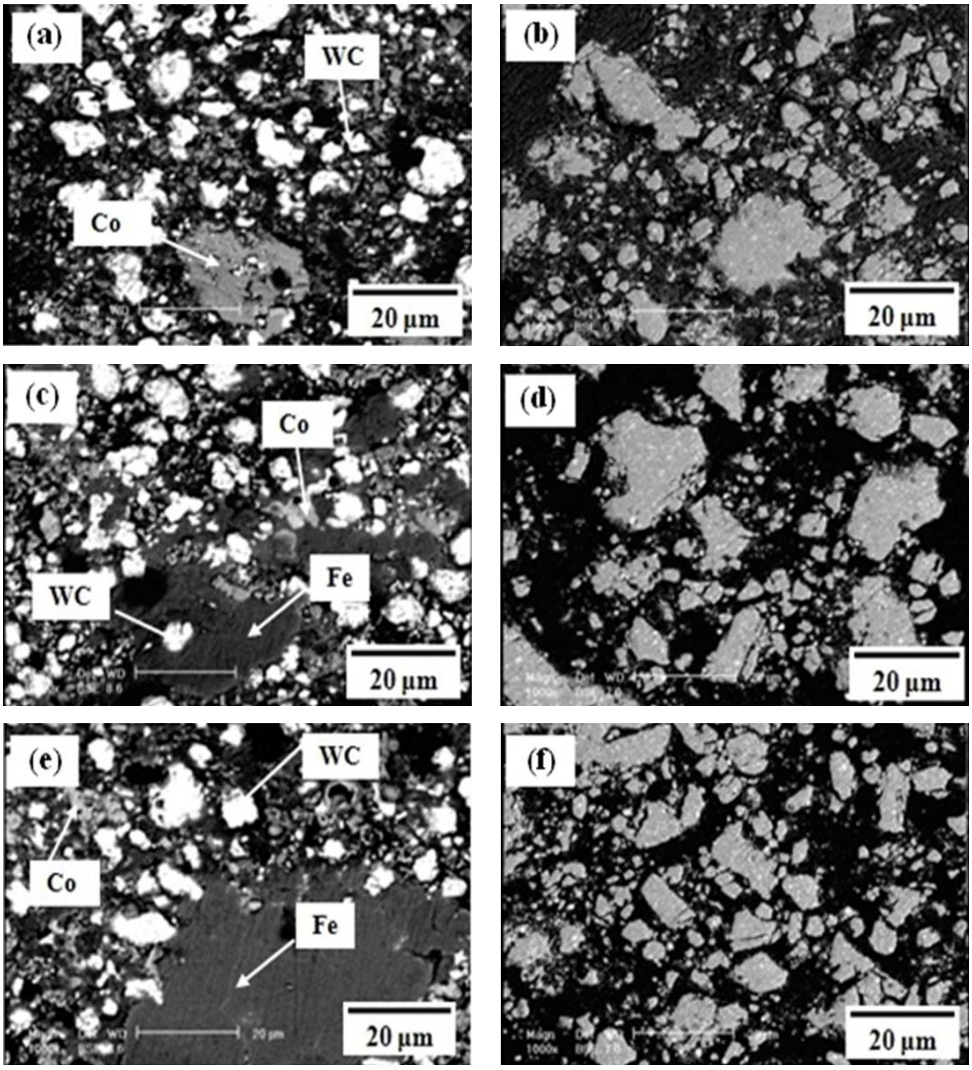

Fig. 8. Cross-sectional BSE-SEM micrographs of the powder particles of the samples (a) A1, (b) A2, (c) B1 (d) B2, (e) D1, and (f) D2

Table 2. Sample codes after sintering of the milled powders

Sample code	Milling time	Composition
A1	15 min	A: Co-80%WC
A2	25 hr	
B1	15 min	B: Fe/Co: 2/8 – 80% WC
B2	25 hr	
C1	15 min	C: Fe/Co: 1/1 – 80% WC
C2	25 hr	
D1	15 min	D: Fe/Co: 7/3 – 80% WC
D2	25 hr	

milling time for each sample leads to increase in the relative density.

Morphology of the milled powders after 15 min and 25 h MA is presented in Fig. 10. It is evident that the milled powders after 25 h of milling are agglomerated. There are considerable differences between powders where each individual powder particle is neighbor-free and -independent and those in which the primary particles, or crystallites, are

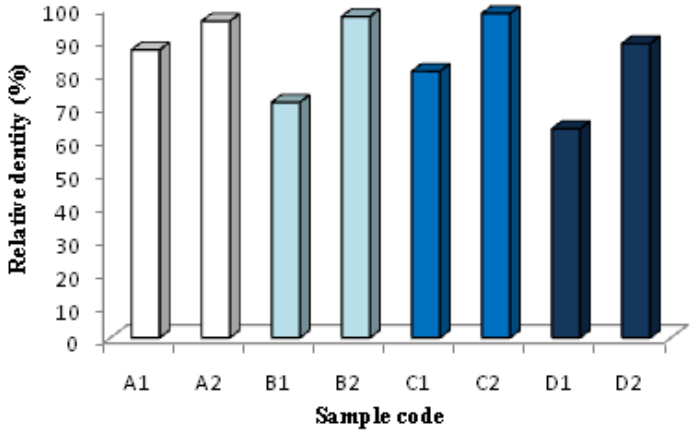

Fig. 9. Relative density of the sintered composites after 15 min and 25 h of milling

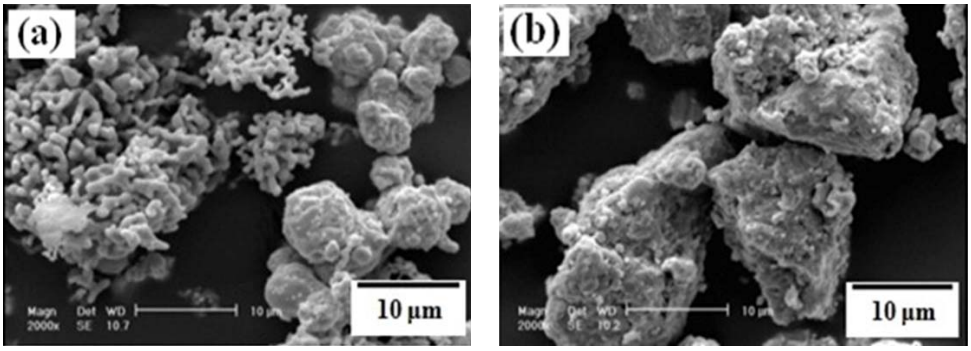

Fig. 10. Morphology of the milled powders after (a) 15 min and (b) 25 h of milling

chemically or physically bonded together to form larger units, are termed agglomerates or aggregates [24]. Therefore, a mixture of agglomerated powder can be effective to increase the density and sintering ability [24].

As the utmost homogeneity in WC grain size and its distribution in the binder are a prerequisite for all cemented carbides, the effect of the MA time on the microstructure of the samples, after sintering at 1350 ° C, is presented in Fig. 11. The most noticeable features of the micrographs are distribution of WC in the binder and the porosity size. In the microstructure of the sintered samples, after physical mixing (15 min of milling), large porosity can be seen. Furthermore, the distribution of the carbide phase in the binder is not homogeneous and binder pooling is observed caused by non-uniform distribution of the binder during milling [25, 26]. The existence of the porosity confirms lower relative density of the sintered samples after physical mixing (Fig. 9) .On the other hand, in sintered samples after 25 h of milling, tungsten carbide grains have a uniform distribution with a lower grain size. Moreover, the porosity level is very low or negligible.

Fig. 12 shows the results of the samples hardness after sintering at 1350°C. As can be seen, with the increase of milling time in all samples, hardness increases. Generally, hardness of the cemented carbides is affected by different parameters such as the amount and type of the binder, size, distribution, and the contiguity of the carbide phase and porosity [27-29]. With the decrease of the WC grain size, the hardness of the WC-based cemented carbides increases according to the Hall-Petch relationship formulated as follows:

$$H = H_o + K_y d^{-1/2} \quad [2]$$

Where H is the hardness of the alloy, d is the mean WC grain size, H_0 and K_y are functions of the properties of the individual phases, of the composition and of the microstructural parameters of the alloy [30].

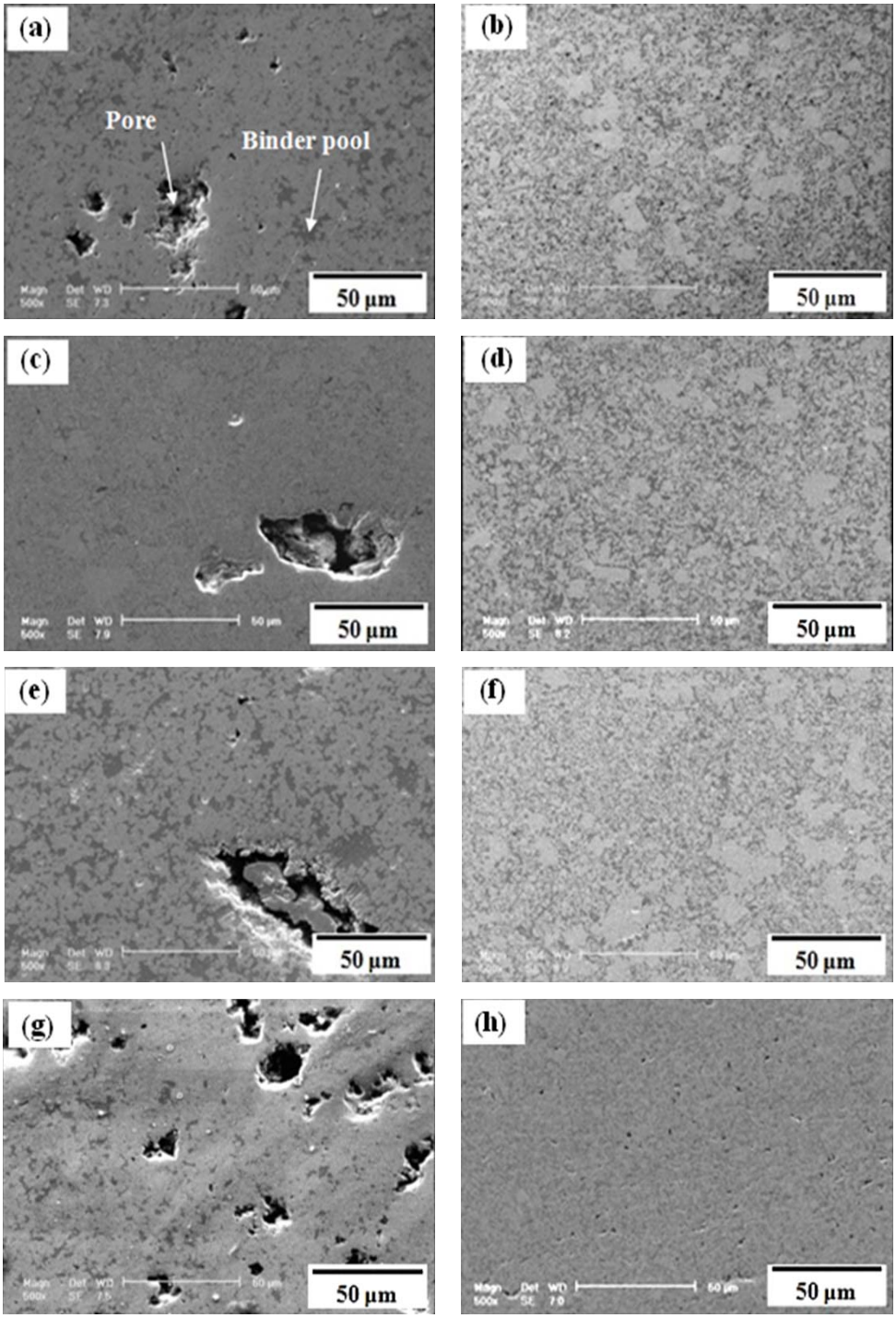

Fig. 11. SEM micrographs of the sintered samples after different milling times, (a) A1 (b) A2, (c) B1 (d) B2, (e) C1, (f) C2, (g) D1,and (h) D2

The average WC grain size, measured by the following linear-intercept equations using stereological principles, is shown in Table 3.

$$L = \frac{2V_{WC}}{2N_{CC} + N_{BC}} \quad [3]$$

where L is the average carbide grain size, V_{WC} is the Volume fraction of WC phase, and N_{CC} and N_{BC} are the average numbers of intercepts per unit length of test line with traces of carbide/carbide boundary and binder/carbide interface, respectively [31]. The values in

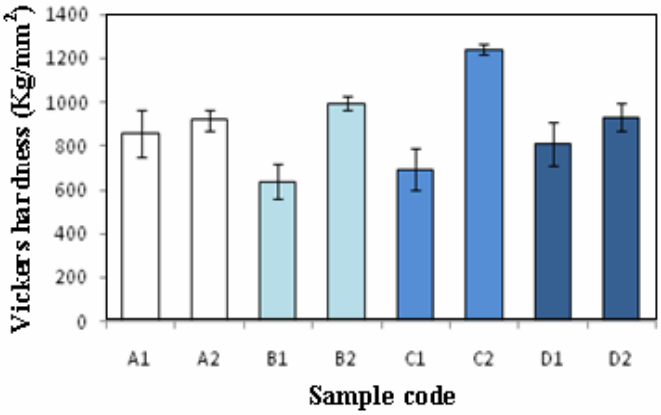

Fig. 12. Hardness of the samples after sintering at 1350˚C

Table 3. The average WC grain size, measured by linear-intercept method

Sample code	Grain size (μm)
A1	2.95 (1.48)*
A2	1.7 (1.05)
B1	2.55 (1.25)
B2	1.51 (0.79)
C1	2.1 (1.1)
C2	1.01 (0.94)
D1	2.23 (1.06)
D2	2.15 (1.02)

∗ The values in parentheses denote standard deviations in the measurements.

parentheses denote standard deviations in the measurements.

4. Conclusions

Fe, Co and WC powders with different ratios of iron to cobalt were milled at different milling times (15 min, 5 h, 10 h and 25 h) to obtain the nanostructured WC-20 wt.% (Fe,Co) composites. In different ratios of iron to cobalt, a homogeneous distribution of nanostructured WC in the binder matrix was formed after 25 h of milling. In order to investigate the sintering behavior of the milled powders (15 min and 25 h), conventional sintering at 1350˚C was performed. Increasing the milling time for each sample led to increase in the relative density and hardness due to grain size reduction. Optimum levels of densification and hardness were obtained for 25 h of milling with equal ratio of iron to cobalt with 98.2% and 1241 HV_{30}, respectively.

Acknowledgement

The authors are grateful for support of this research by Isfahan University of Technology.

References

1. S. A. Hewitt, K. A. Kibble, “Effects of ball milling time on the synthesis and consolidation of nanostructured WC–Co composites”, Int. J. Refract. Met. Hard. Mater., Vol. 27, 2009, pp. 937-48.
2. Y. Wang, Z. Xu, “Nanostructured Ni–WC–Co composite coatings fabricated by electrophoretic deposition”, Surf. Coat. Tech., Vol. 200, 2006, pp. 3896-902.
3. F. L. Zhang, C. Y. Wang, M. Zhu, “Nanostructured WC/Co copmposite powder prepared by high energy ball milling”, Scripta.

Mater., Vol. 49, 2003, pp. 1123-28.
4. B. Wittmann, W. D. Schubert, B. Lux, "WC grain growth and grain growth inhibition in nickel and iron binder hard metals", Int. J. Refract. Met. Hard. Mater., Vol. 20, 2002, pp. 51-60.
5. G. S. Upadhyaya, S. K. Bhaumik, "Sintering of submicron WC-10wt.%Co hard metals containing nickel and iron", Mater. Sci. Eng., Vol. A105/106, 1988, pp. 249-56.
6. J. M. Guilemany, I. Sanchiz, B. G. Mellor, N. Llorca, J. R. Miguel, "Mechanical-property relationships of Co/WC and Co-Ni-Fe/WC hard metal alloys", Int. J. Refract. Met. Hard. Mater., Vol. 12, 1993-1994, pp. 199-206.
7. R. Subramanian, J. H. Schneibel, "Intermetallic bonded WC-based cermets by pressureless melt infiltration", Intermetallics, Vol. 5(5), 1997, pp. 401-8.
8. M. Ahmadian, D. Wexler, T. Chandra, A. Calka, "Abrasive wear of WC–FeAl–B and WC–Ni_3Al–B composites", Int. J. Refract. Met. Hard. Mater., Vol. 23, 2005, pp. 155-59.
9. T. Farooq, T. J. Davies, "Tungsten carbide hard metals cemented with ferroalloys", Int. J. Powder. Metall., Vol. 27, 1991, pp. 347-55.
10. B. J. Marques, C. M. Fernandes, A. M. R. Senos, "Sintering, microstructure and properties of WC-AISI304 powder composites", J. Alloy. Compd., Vol. 562, 2013, pp. 164-170.
11. L. Prakash, Development of tungsten carbide hard metals using iron-based binder alloys, Ph.D. Thesis, Institute for Material and Solid State Research, Kernforschungszentrum, 1980.
12. C. Hanyaloglu, B. Aksakal, J. D. Bolton, "Production and indentation analysis of WC/Fe-Mn as an alternative to cobalt-bonded hard metals", Mater. Charact., Vol. 47, 2001, pp. 315-22.
13. T. W. Penrise, "Alternative binders for hard metals", J. Mater. Shap. Tech., Vol. 5, 1987, pp. 35-9.
14. I. J. Shon, I. K. Jeong, I. Y. Ko, J. M. Doh, K. D. Woo, "Sintering behavior and mechanical properties of WC–10Co, WC–10Ni and WC–10Fe hard materials produced by high-frequency induction heated sintering", Ceram. Int., Vol. 35, 2009, pp. 339-44.
15. H. R. de Macedo, A. G. P. da Silva, D. M. A. de Melo, "The spreading of cobalt, nickel and iron on tungsten carbide and the first stage of hard metal sintering", Mater. Lett., Vol. 57 (24–25), 2003, pp. 3924-32.
16. C. M. Fernandes, A. M. R. Senos, "Cemented carbide phase diagrams: A review", Int. J. Refract. Met. Hard. Mater., Vol. 29(4), 2011, pp. 405-18.
17. V. K. Portnoi, K. V. Tetyakov, V. I. Fadeeva, "Structural transformations during the mechanochemical synthesis and heating of Co-Al alloys", Inorg. Mater., Vol. 40, 2004, pp. 937-44.
18. Y. Kimura, H. Kuriyama, T. Suzuki, Y. Mishima, "Microstructure control and mechanical properties of binary Co-Al alloys based on B2 intermetallic compound CoAl", Mater. Trans. JIM., Vol. 35, 1994, pp. 182-8.
19. J. Li, X. Ni, G. Wang, "Microstructure and magnetic properties of Co/Al_2O_3 nanocomposite powders", J. Alloy. Compd., Vol. 440, 2007, pp. 349-356.
20. Y. D. Kim, J. Y. Chung, J. Kim, H. Jeon, "Formation of nanocrystalline Fe–Co powders produced by mechanical alloying", Mater. Sci. Eng., Vol. A291, 2000, pp. 17-21.
21. H. Moumenia, S. Alleg, J. M. Greneche, "Structural properties of $Fe_{50}Co_{50}$ nanostructured powder prepared by mechanical alloying", J. Alloy. Compd., Vol. 386, 2005, pp. 12-19.
22. G. K. Williamson, W. H. Hall, "X-ray line broadening from filed Aluminum and Wolfram", Acta. Metall., Vol. 1, 1953, pp. 22-31.
23. C. Suryanarayana, "Mechanical alloying and milling", Prog. Mater. Sci., Vol. 46, 2001, pp. 1-184.
24. M. J. Mayo, D. J. Chen, D. C. Hague, "Consolidation of nanocrystalline materials by compaction and sintering", in: Nanomaterials. Synthesis, Properties and Applications, Institute of Physics Publication, Philadelphia, 1997, pp. 165-197.
25. R. M. Genga, L. A. Cornish, G. Akdogan, "Effect of Mo_2C additions on the properties of SPS manufactured WC–TiC–Ni cemented carbides", Int. J. Refract. Met. Hard. Mater., Vol. 41, 2013, pp. 12-21.
26. S. Amberg, H. Doxner, "Porosity in cemented carbides", Powder. Metall., Vol. 20(1), 1977, pp. 1-10.
27. C. S. Kim, T. R. Massa, G. S. Rohrer, "Modeling the relationship between microstructural features and the strength of WC–Co composites", Int. J. Refract. Met. Hard. Mater., Vol. 24, 2006, pp. 89-100.
28. H. C. Lee, J. Gurland, "Hardness and deformation of cemented tungsten carbides", Mater. Sci. Eng., Vol. 33, 1978, pp. 125-133.
29. S. Cha, K. Lee, H. Ryu, S. Hong, "Analytical modeling to calculate the hardness of ultra-fine WC-Co cemented carbides", Mater. Sci. Eng., Vol. A489, 2008, pp. 234-44.
30. Y. V. Milman, S. Luyckx, I. T. Northrop, "Influence of temperature, grain size and cobalt

content on the hardness of WC-Co alloys", Int. J. Refract. Met. Hard. Mater., Vol. 17, 1999, pp. 39-44.

31. C. S. Kim, T. R. Massa, G. S. Rohrer, "Interface character distributions in WC–Co composites", J. Am. Ceram. Soc., Vol. 91(3), 2008, pp. 996-1001.